Energy Storage Materials 12 (2018) 204–215

Contents lists available at ScienceDirect

Energy Storage Materials

journal homepage: www.elsevier.com/locate/ensm

Supercapacitors based on AC/MnO_2 deposited onto dip-coated carbon nanofiber cotton fabric electrodes

A.J. Paleo[a,*], P. Staiti[b], A. Brigandì[b], F.N. Ferreira[a], A.M. Rocha[a], F. Lufrano[b,*]

[a] University of Minho, Department of Textile Engineering, Centre for Textile Science and Technology (2C2T), Campus de Azurém, 4800-058 Guimarães, Portugal

[b] CNR-ITAE, Istituto di Tecnologie Avanzate per l'Energia "Nicola Giordano", 98126S. Lucia, Messina, Italy

ARTICLE INFO

Keywords:
Supercapacitor
Carbon nanofiber
Manganese oxide
Solid-state
Hybrid supercapacitors

ABSTRACT

This work introduces the preparation of flexible carbon composite electrodes based on the top-down approach starting from the dip-coating of carbon nanofibers (CNFs) onto a cotton fabric. On these so-obtained conductive cotton fabrics, further layers of activated carbon and manganese oxide (MnO_2) materials were subsequently added to enhance the electrochemical performances of negative and positive electrodes. At the end, two different types of asymmetric supercapacitors (SCs) were assembled with those textile electrodes by using porous paper and Nafion-Na ion-exchange membranes as separators. The different SCs were electrochemically characterized by means of cyclic voltammetry (CV), galvanostatic charge/discharge (G–CD) and electrochemical impedance spectroscopy (EIS). These hybrid carbon-based textile SCs exhibited capacitance performance of 138 and 134 F g^{-1} with the porous paper and Nafion membrane, respectively, and low self-discharge rates. Furthermore, in this study is considered the combination of two methods (cycling and floating) for studying the long-term durability tests of SCs. In particular, the floating methodology utilizes much more harsh conditions than the common cycling based on G-CD tests at high currents usually discussed in literature. The solid-state (Nafion membrane) hybrid device demonstrated very long durability with 10 K cycles and additional 270 h at a constant voltage of 1.6 V. In summary, the hybrid SCs fabricated with low cost materials and simple methodologies reported in this study showed very promising results for flexible energy storage applications.

1. Introduction

Electrochemical supercapacitors (SCs), consisting of two electrodes, an electrolyte and a separator, are promising energy storage devices because they store much more energy than traditional capacitors and deliver higher power than batteries and fuel cells; they store and deliver energy quickly and for many thousand cycles without performance decaying; they have high current charge-discharge capabilities and high power densities; they are environmentally safe under extreme conditions and they work well over a wide temperature range [1–3]. In SCs it is generally accepted that energy is electrostatically stored by accumulated charges on the electrode surface, and electrolyte ions with counterbalancing charge on the electrolyte side, which is denominated as electric double layer capacitance [4]. On the other hand, it is well known that, in electrical double layers, charges can be increased with pseudocapacitive processes consisting of highly reversible surface redox reactions which sometimes are ruled by concomitant processes of intercalation-deintercalation or by electrosorption of chemical species on surface of carbon materials, conducting polymers and transition metal oxides [5]. Among pseudocapacitive materials, transition metal oxides such as manganese oxides (MnO_x) are very promising, because their high redox reversibility, fast diffusion performance, cost-effective and environmentally friendly properties [6,7]. The charge storage mechanism of manganese oxide based electrodes is mainly related to faradaic reactions due to the shuttle redox reactions between Mn (IV) and Mn (III) in outer active surface sites, which are promoted through the insertion of electrolyte cations and protons [8,9]. Furthermore, an asymmetric supercapacitor formed with MnO_2 based materials at positive electrode and carbon material at negative electrode, show enhanced energy density compared to symmetric supercapacitors based only on carbon materials [10].

Also, the recent rise in wearable technologies is demanding the development of novel energy storage devices able to provide power with specific properties such as high stability, low cost and high mechanical flexibility [11–14]. Hence, fabrics, which are thin flexible sheets of interlaced yarns produced by different technologies such as weaving, knitting, and braiding have additional advantages over other materials owing to their mechanical strength, flexibility properties and

* Corresponding authors.
E-mail addresses: ajpaleovieito@2c2t.uminho.pt (A.J. Paleo), lufrano@itae.cnr.it (F. Lufrano).

https://doi.org/10.1016/j.ensm.2017.12.013
Received 21 November 2017; Received in revised form 13 December 2017; Accepted 13 December 2017
Available online 18 December 2017

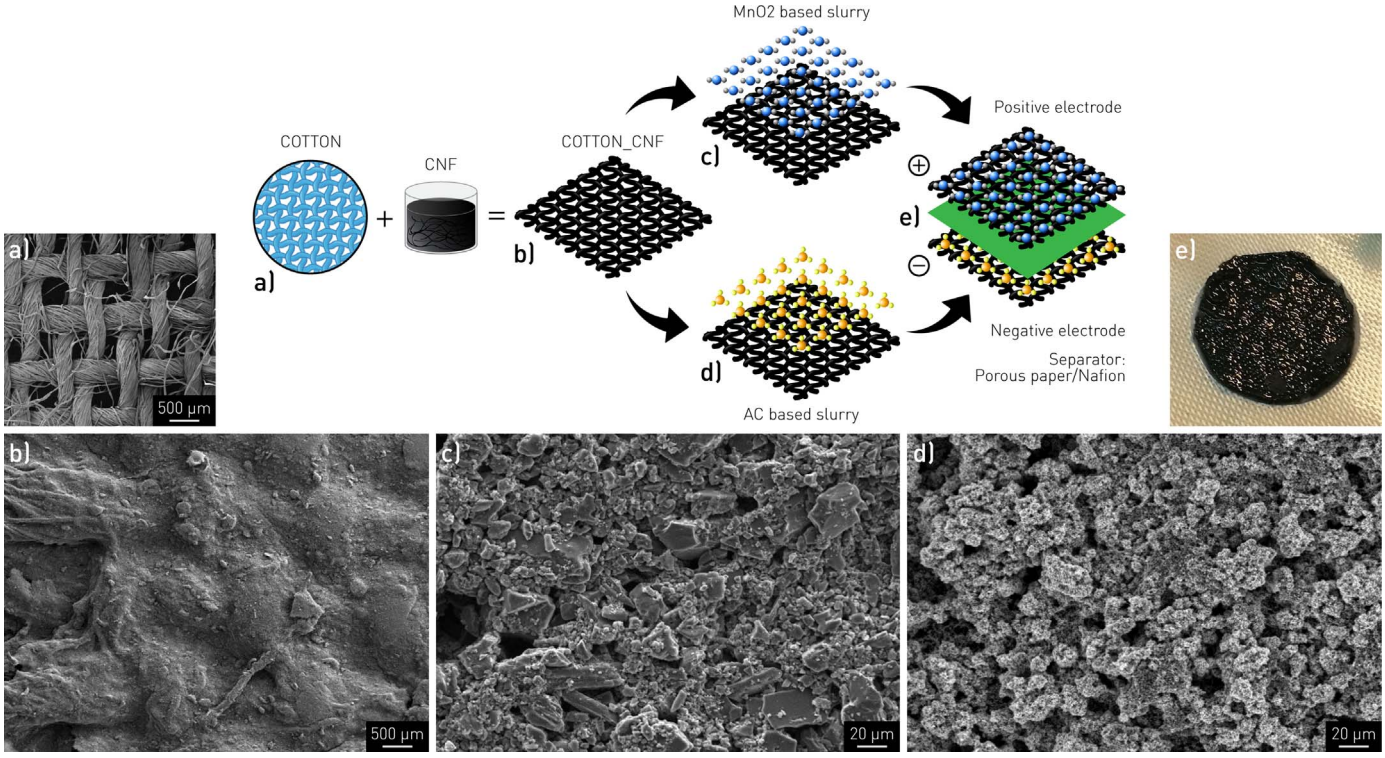

Fig. 1. Schematic design of positive and negative electrodes and final assembled SC (a–e); (a) SEM image of 100% cotton woven fabric; (b) Dip-coated fabric sample (Cotton_CNF); (c) SEM image of top MnO_2 electrode; (d) SEM image of top AC electrode (e) digital image of hybrid composite supercapacitor (Cotton_CNF@/Nafion SC).

absorption and desorption ability (for absorbing and releasing of ions in solvent content) [15]. Among natural fiber fabrics, the cotton-based, are drawing strong attention to act as wearable platform for textile supercapacitors [16]. The current research in the development of textile supercapacitors can be separated into two main lines of investigation, bottom-up and top-down, as established in a recent review [15]. In the bottom-up approach, natural or synthetic fibers are transformed into electrode fibers by different methodologies, such as carbonization, so they can be interlaced in a subsequent step to produce energy storage devices [17,18]. On the contrary, the top-down approach transforms already produced fabrics into energy storage devices. This latter approach generally utilizes a two-step process due to the electrically insulating properties of fabrics. In the first step, fabrics are coated with a layer of conductive materials, whereas in the second step, diverse active materials are deposited by means of different methodologies onto the surface of those already conductive fabrics to achieve higher capacitive performances [15].

The first work reporting this type of top-down approach with cotton fabric has been conducted by Yi Cui research group in 2010 [19]. In their work, ink of single wall carbon nanotubes (SWCNT) was dip-coated onto the fabric and tested as electrodes in supercapacitors with a cotton fabric impregnated with 2 M Li_2SO_4, as separator. Capacitances of around 50 F g^{-1} were measured at a current density of 2 mA cm^{-2}. In the same work, supercapacitors based on electro-deposited MnO_2 on the same SWCNT/Cotton electrodes were developed and tested in a working voltage range of 0.8 V with values of around 125 F g^{-1} at the same current density. Such wearable SCs showed excellent cycling stability with 100% of specific capacitance retention over 35 K cycles. In another very complete work, commercial activated carbon (AC) was dip-coated onto a cotton woven fabric, and then a slurry containing another kind of commercial AC was deposited by screen-printing, whereas PTFE porous membrane impregnated with 1 M Na_2SO_4 and 2 M Li_2SO_4 solutions was used as separator. At the end, SCs tested in the working voltage range of 1 V with the two different electrolytes showed values of specific capacitance of 85 and 90 F g^{-1} at 0.25 A g^{-1}, respectively, and a specific capacitance retention of 92% over 10 K cycles [20]. Another work reported the use of cotton cloth as platform for electrodes by “brush-coating and drying” of a stable graphene oxide (GO) suspension followed by annealing at 300 °C in argon atmosphere. By using these electrodes, cotton cloth as separator, and 6 M KOH as electrolyte in the working voltage range of 1 V, a specific capacitance of 81.7 F g^{-1} at 10 mV s^{-1} was achieved, whereas a specific capacitance retention of 94% over 1.5 K cycles was reported. SCs in this work achieved an energy density of 7.13 Wh kg^{-1} [21]. More recently, graphene nanosheets/nickel sulfide based materials were prepared by dip and dry and electrodeposition methods onto commercial make-up cottons [22]. The hybrid electrode yielded a specific capacitance of 775 F g^{-1} for a potential range of only 0.4 V at a charge/discharge specific current of 0.5 A g^{-1} with 6 mol L^{-1} KOH as electrolyte by testing with the three-electrode cell configuration. A capacitance retention of 88.1% after 1 K cycles at 2 A g^{-1} was also reported. Finally, in another recent work, a nickel coated cotton fabric, via polymer-assisted metal deposition, was prepared, followed by MWCNT and reduced graphene oxide (rGO) deposition by vacuum filtration. This investigation achieved a specific capacitance of 262 F g^{-1} at 0.84 A g^{-1} in the working voltage range of 0.8 V by using cotton fabric as separator sandwiched between two symmetric electrodes in 5 M LiCl aqueous electrolyte solution. These SCs achieved also an unexpected increment of 18% in their specific capacitance after 10 K cycles [23].

In summary, the above-mentioned research works inspired by the combination of different carbon structures and metal oxide materials onto cotton substrates are just a proof of the current interest in integrating textiles as electrodes for the next generation of flexible energy storage devices [24–29]. Likewise, in this work, electrically conducting electrodes have been produced by the dip and dry coating method of carbon nanofibers (CNF) onto cotton woven fabrics (Fig. 1b). Subsequently, in a second step, hybrid electrodes based on manganese oxide materials for the positive electrodes (as shown in Fig. 1c) and activated carbon (AC) materials for the negative electrodes

Table 1
Constructional parameters and physical properties of the cotton woven fabrics being a Porosity (%) = 1- [Fabric density (g/cm^3)/ Fibre density (for cotton, 1.54 g/cm^3)] x 100.

Fabric parameters and properties	
Weave pattern	1/1 plain
Warp × weft yarns linear density (tex)	14.9 × 20.2
Number of warp × weft yarns (cm^{-1})	35.0 × 14.0
Fabric mass (g m^{-2})	93.35
Fabric thickness at 18 Pa (mm)	0.26
Fabric density (g cm^{-3})	0.359
Fabric porosity (%)[a]	76.7

were produced (Fig. 1d). At the end, two different types of asymmetric supercapacitors were assembled and investigated (general scheme and Fig. 1e). The first type consisting of those electrodes and porous paper separator, whereas the second type was assembled by using the same electrodes with Nafion-Na ion-exchange membrane. Both types of SCs were electrochemically characterized by cyclic voltammetry (CV), galvanostatic charge/discharge (G–CD), electrochemical impedance spectroscopy (EIS) and long-term durability tests.

2. Experimental section

2.1. Materials

As base-substrate of the electrodes, a 100% cotton woven fabric was used. The constructional parameters and physical properties of the fabric are listed in Table 1. Vapor grown carbon nanofibers (CNF), Pyrograf III PR 24 LHT XT, (ASI, Cedarville, OH, USA), were used to provide electrical conducting properties to the fabric. PR 24 LHT XT fibers have an average outer diameter of 100 nm with an average bulk density ranging from 0.032 to 0.064 g cm^{-3} and a highly graphitic outer wall layer. This particular grade (LHT) is treated at 1500 °C.

A combination of activated carbon with a specific surface area of 1500 m^2 g^{-1} (Norit A Supra Eur), graphite fibres, carbon black (Shawinigan acetylene black), and dry powder manganese oxide, this latter prepared by a simple method based on chemical reaction in aqueous solution [10], was used for producing the active layers. Porous paper separator (Nippon Kodoshi Corportion, Japan) embedded of 1 M Na_2SO_4 with a thickness of 60 μm, and sodium exchanged polymer membrane (Nafion 115, 150 μm, DuPont), were employed as separator and solid-state electrolyte, respectively. All the other materials used in this work were purchased from Sigma-Aldrich and used without further purification.

2.2. Preparation of electrodes and supercapacitors

First, 5 mg ml^{-1} sodium dodecylbenzenesulfonate (SDBS) surfactant was dissolved in distilled water. A concentration of 6.4 mg ml^{-1} CNF were then added to the surfactant solution; after this, the CNF solution was dispersed through tip sonication (ultrasonic homogenizer CY-500; 60% power, 5 min) to prepare CNF ink. A series of 100% cotton woven fabric samples (2 × 2 cm^2) were dipped individually in 60 ml of this CNF ink for 5 min and dried after in an oven for 10 min at 80 °C. This process was repeated five times. These dip-coated fabric samples will be named as Cotton_CNF in the remainder of this study.

Second, the carbon-based active layers for the negative electrodes were prepared by spreading onto the Cotton_CNF samples a slurry consisting of: 90 wt% of activated carbon (AC); 5 wt% of graphite fibres; 5 wt% of poly(vinylidene fluoride) (PVDF) binder; and N,N dimethylacetamide (DMA) solvent. Whereas the MnO_2-based active layers for the positive electrodes were prepared by spreading onto the Cotton_CNF samples a slurry composed of: 70 wt% of MnO_2, 10 wt% of carbon black, 10 wt% of graphite fibers, 10 wt% of PVDF and DMA. Both types of hybrid electrodes were dried at 70 °C for 18 h, after which, a further heat treatment of 1 h at 120 °C was carried out to improve their mechanical strength. The thicknesses of top active layers were 120 ± 20 μm and 130 ± 20 μm for MnO_2 positive and AC negative electrodes, respectively.

Third, one positive and one negative electrodes were assembled with the porous paper separator for preparing the first type of hybrid asymmetric SC, which was named as Cotton_CNF@/Paper (where @ represents the active added layers), and other positive and negative electrodes were assembled with the sodium exchanged membrane for preparing the second type of hybrid asymmetric SC developed in this study, which was named as Cotton_CNF@/Nafion. All electrodes were cut with circular shapes and areas of 2 cm^2, whereas paper separator and Nafion 115 membrane were cut slightly larger than 2 cm^2 to prevent lateral short circuits. All of them were impregnated before assembling with 1 M Na_2SO_4. For the solid-state Cotton_CNF@/Nafion supercapacitor, the Nafion 115 membrane was exchanged in Na^+ form by treatment with 1 M Na_2SO_4 (18 h) under slow stirring. At the end, the loading of active layers based on MnO_2 was 3.22 mg cm^{-2} for Cotton_CNF@/Paper SC and 2.87 mg cm^{-2} for Cotton_CNF@/Nafion SC; whereas the loading of active layers based on AC was 2.83 mg cm^{-2} for Cotton_CNF@/Paper SC and 3.15 mg cm^{-2} for Cotton_CNF@/Nafion SC. A reference symmetric supercapacitor, called Cotton_CNF/Paper, consisting of two identical Cotton_CNF samples as electrodes and porous paper separator was assembled for comparative purposes. A more detailed description of the final produced solid-state SCs is listed in Table 2.

2.3. Morphological characterization

Morphological analysis of as base-substrate 100% cotton woven fabric and dip-coated fabric samples Cotton_CNF was realized in an Ultra-high resolution Field Emission Gun Scanning Electron Microscopy (FEG-SEM), NOVA 200 Nano SEM, FEI Company. Secondary electron images to analyze the topography of samples, at different step of electrode preparation, were performed at various acceleration voltages. Samples were covered with a thin film (20 nm) of Au-Pd (80-20 wt%) in a high resolution sputter coater, 208 h Cressington Company, coupled to a MTM-20 Cressington High Resolution Thickness Controller.

2.4. Electrical resistivity

Electrical resistivity of Cotton_CNF samples was measured by using the conventional four probe van der Pauw method. Four different resistances (R_s) were measured by changing the probes used for the

Table 2
List of investigated solid-state supercapacitors.

Supercapacitor name	Positive electrode	Negative electrode	Separator	Electrolyte
Cotton_CNF/Paper	Cotton_CNF	Cotton_CNF	Porous paper separator	1 M Na_2SO_4
Cotton_CNF@/Paper	Cotton_CNF + MnO_2 layer [70% MnO_2, 10% CB, 10% GF, 10% PVDF]	Cotton_CNF + AC layer [90% AC, 5% GF, 5% PVDF]	Porous paper separator	1 M Na_2SO_4
Cotton_CNF@/Nafion	Cotton_CNF + MnO_2 layer [70% MnO_2, 10% CB, 10% GF, 10% PVDF]	Cotton_CNF + AC layer [90% AC, 5% GF, 5% PVDF]	Nafion membrane	1 M Na_2SO_4

current supplying and voltage measurement. The final value of resistivity $\rho = Rs\ d$, where d is the thickness of the Cotton_CNF sample, was calculated as the average of five measurements per sample.

2.5. Electrochemical characterization of SCs

A three-electrode cell was used to study separately the capacitive properties of positive and negative electrodes of solid-state supercapacitors through cyclic voltammetry measurements carried out at the voltage sweep rate of 5 mV s^{-1} and at variable potential ranges.

The 2 cm^2 circular-shape two-electrode supercapacitors were investigated in a titanium cell connected to Autolab/Methrom PGSTAT 302/FRA2 (Eco Chemie, Netherlands) potentiostat. At the same time, a second equipment (Multifunction Datalogger - Delta OHM, Italy) connected with the same titanium cell, which used a saturated calomel electrode (SCE) in contact with the membrane/separator of supercapacitors, was also used to monitor the potentials of single electrodes [10]. Cyclic voltammetry (CV) was carried out in potentiodynamic mode at different voltage sweep rates (5, 10, 20, 40 mV s^{-1}) and voltage range from 0 to +1.6 V and vice versa. Galvanostatic charge/discharge (G-CD) was carried out in the same voltage range (0 to +1.6 V) and constant currents of ± 0.2, ± 0.5, ± 1 and ± 2 A g^{-1}.

Electrochemical impedance spectroscopy (EIS) was performed at open circuit voltage (OCV), with 5 mV in amplitude, and frequencies from 1 mHz to 500 kHz by using the PGSTAT 302 potentiostat equipped with a FRA2 module.

2.6. Accelerated ageing method of SCs

We propose a new method to assess the long-term durability of supercapacitors. This method allows the monitoring of the aging behavior of supercapacitors through a procedure of cycling and floating, which can better simulate the lifetime and durability behavior of supercapacitors, for the prediction of their state-of-health (SoH). This method is harsher than the usual cycling G-CD tests performed at high currents [10,30,31]. In particular, SCs during floating tests are maintained at maximum voltage of 1.6 V for long periods of time. This accelerated aging method begins with control tests (CV at 10 mV s^{-1}, G-CD at 0.5 A g^{-1} and EIS measurements) to determinate the initial electrochemical features such as resistance and capacitance of the capacitor, after which sequences of G-CD cycles at 2 A g^{-1} are programed. Subsequently, new control tests are carried out for 1000, 2000 and up to 10 K cycles, with the same conditions for CV (10 mV s^{-1}), G-CD (0.5 A g^{-1}) and EIS. The G-CD cycling procedure is continued until 10 K cycles at 2 A g^{-1}. Then, the supercapacitor is subjected to periodic floating tests at the maximum voltage of 1.6 V with new control tests programed for 25, 50, 70, 120, 200 and 270 h (CVs at 10 mV s^{-1}, GCDs 0.5 A g^{-1}, EIS). At the end, both Cotton_CNF@/Paper and Cotton_CNF@/Nafion SCs, were tested to G-CD 10 K cycles and 270 h of floating test to monitor their aging behavior.

2.7. X-ray photoelectron spectroscopy

The post-mortem x-ray photoelectron spectroscopy (XPS) analysis of fresh and aged electrodes of Cotton_CNF@/Nafion and Cotton_CNF@/Paper SCs was performed by using a Physical Electronics (PHI) 5800-01 spectrometer. Spectra was obtained by using pass energies of 58.7 eV, for elemental analysis, and 11.75 eV for the determination of oxidation states and chemical compositions. A survey scan for each sample, obtained by generating a spectrum from 0 eV to 1200 eV, was used to determine the elemental composition in the surface. High-resolution scans were obtained for Mn 2p, C 1s and O 1s. Different carbon and MnO_x samples were calibrated with C 1s (284.8 eV) peak. The areas of peaks were estimated by calculating the integral of each peak after subtraction of the background and fitting the experimental peak by Gaussian curve.

3. Results and discussion

3.1. Morphological analysis

The Scanning Electron Microscopy observations of dip-coated fabric samples or Cotton_CNF shown in Fig. 1b demonstrate that a layer of CNF of approximately 30–40 μm in thickness was successfully coated onto cotton woven fabric. Compared to other grades of Pyrograf III, the PR 24 HT XT grade has higher aspect ratio than other grades such as PR 25 PS XT which would help to make better ink dispersions [32]. This grade also has better intrinsic conductivity. Accordingly, the electrical resistivity of the Cotton_CNF samples was 0.64 ± 0.03 Ω cm (Fig. 1c). Further, SEM image of MnO_2 coated on cotton fibers is shown in Fig. 1c and the respective image of AC in Fig. 1d. SEM images in Fig. 1(c–d) display that the obtained MnO_2 and AC active layers exhibit a homogeneous particles dispersion that coats uniformly the Cotton_CNF fabric. Besides, the top view SEM image shows that the micron-size particles of AC (Fig. 1d) are smaller than that MnO_2 (Fig. 1c) with a good interconnection between different materials (e.g. MnO2, carbon black, graphite fibers and PVDF binder), that facilitates the electronic path.

3.2. Electrochemical characterization of SCs

The positive and negative electrodes were studied separately in the three-electrodes cell configuration through cyclic voltammetry measurements at voltage sweep rate of 5 mV s^{-1}. The results of the test, with data of current converted in capacitance, are reported in Fig. 2. The voltammograms display quasi-rectangular shapes with near mirror image symmetry showing similar capacitances between the charging and discharging features of both positive and negative electrodes. The curves denote the absence of redox peaks and irreversible processes in the range 0 to +1 V (versus NHE) and 0 to ~ −0.9 V for the manganese oxide (positive scan) and activated carbon electrode (negative scan), respectively. Apparently, there are not redox peaks in the range of voltage investigated for the positive electrode, even if variations of oxidation state of MnO_2 normally occur in this range. Similar results were reported in literature by Demarconnay et al. [33] and by Khomenko et al. [30].

Fig. 3 shows the specific capacitance versus cell voltage, obtained by CV, of the different solid-state hybrid SCs at different voltage sweep rates from 5 to 40 mV s^{-1}. The original values of current in CV plots were converted in capacitance per mass one electrode by using the equation C (F g^{-1}) = [(I (A)/dV dt^{-1} (V s^{-1})]/mass capacitor (g)] × 4; where dV/dt is the scan rate and I is the current. In this figure, the plots related to SC made with two identical Cotton_CNF samples, named as Cotton_CNF/Paper, evidence the negligible capacitance of these electrodes without MnO_2 and AC active layers (blue curves in voltammograms Fig. 3). Fig. 3 shows that Cotton_CNF@/Nafion SC has slightly lower capacitance than Cotton_CNF@/Paper SC. Cotton_CNF@/Nafion supercapacitor works efficiently and with specific capacitances above 100 F g^{-1} for a wide range of voltage scan rates. Notwithstanding

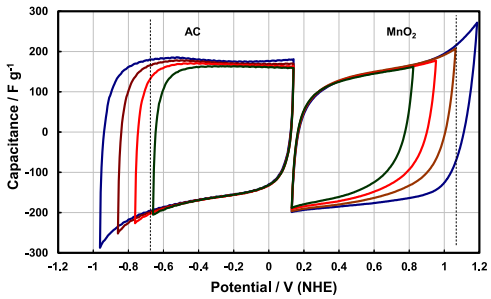

Fig. 2. Comparative voltammograms (CV) of positive (MnO_2) and negative (AC) electrodes at variable potential ranges and scan rate of 5 mV s^{-1}.

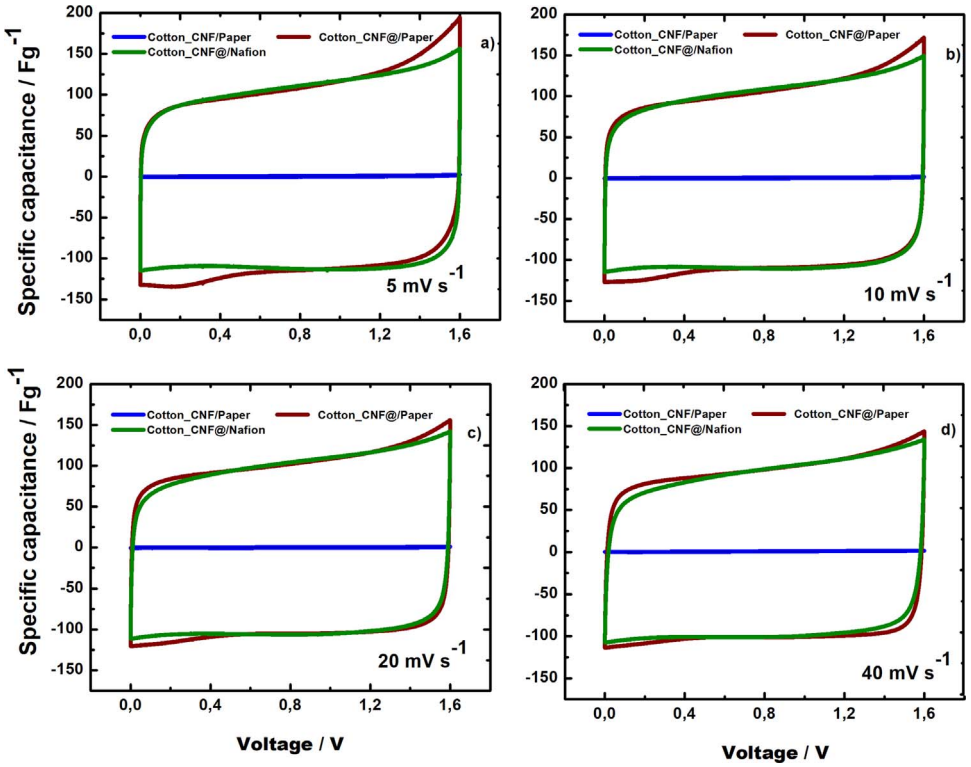

Fig. 3. Specific capacitance versus cell voltage for the different hybrid SCs, at voltage scan rates from 5 mV s^{-1} (a) to 40 mV s^{-1} (d).

Cotton_CNF@/Paper and Cotton_CNF@/Nafion SCs have a high MnO_2 loading in their positive electrodes (≈ 3 mg cm^{-2}), which normally affects the rectangular shape of voltammograms due to Faradaic process, both SCs showed nearly rectangular shapes, with behaviors very similar to a pure capacitor in the voltage range from 0 to +1.6 V. This high voltage (1.6 V) is particularly important because overcomes the thermodynamic potential window of water decomposition at ambient temperature that is 1.23 V and therefore helps to prevent water oxidation phenomena and oxygen and/or hydrogen evolution reactions. These inconveniences are widely investigated in different energy storage devices. For instance, the hydrogen evolution reaction (HER) was suppressed in anode electrodes of lead–acid battery [34,35], where the electrolyte decomposition was kinetically minimized by incorporating suitable inhibitors. On the other hand, the

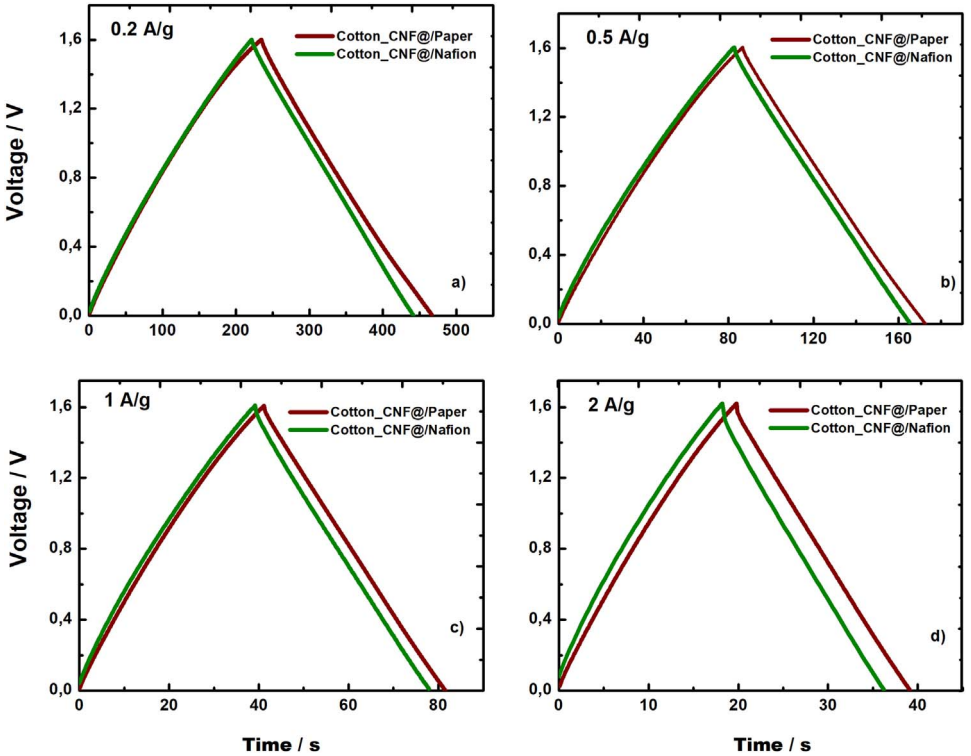

Fig. 4. Galvanostatic charge–discharge curves of Cotton_CNF@/Paper and Cotton_CNF@/Nafion SCs at different current densities from 0.2 A g^{-1} (a) to 2 A g^{-1} (d).

oxygen evolution reaction (OER) and self-discharge rates were minimized by adding inhibitors of OER such as cadmium oxide to the active material in Ni–Cd batteries [36]. In our study, even though water decomposition still could occur due to thermodynamic reasons, there would be the possibility to reduce oxygen/hydrogen evolution reactions from a kinetic point of view, which could allow that supercapacitors could operate with highly concentrated aqueous electrolytes (i.e. water-in-salt) in a wider voltage range under reversible conditions [37]. It was also demonstrated that supercapacitors with MnO_2/carbon capacitors in some neutral aqueous electrolytes (e.g. 1 M Na_2SO_4, 1 M Li_2SO_4 and 1 M KNO_3) can work successfully between 1.6 and 2 V [30,31]. Finally, despite the fact that the investigation of long-term stability, leakage current and self-discharge in a wide voltage window, as it is discussed in this work, is a key feature prerequisite for pre-commercial performance of this type of SCs, it was addressed in very few papers for carbon/carbon supercapacitors [38–40].

Fig. 4 shows galvanostatic charge/discharge curves of Cotton_CNF@/Paper and Cotton_CNF@/Nafion SCs at different discharge currents between 0.2 and 2 A g^{-1} in the potential range from 0 to +1.6 V. All the curves show triangular shapes with low voltage drop (iR drop) at the current inversion, which are associated with the overpotential caused by the electrolyte and electron flow through the electrodes [41]. The low ohmic drops are then connected to the minimization of internal resistances of materials and their interfaces (e.g. electrodes/current collectors). The discharge curve at 2 A g^{-1} shows that the highest ohmic drop is always below few tens of mV and that the resistance values measured at this current are 1.03 and 1.40 Ω cm^2 for the Cotton_CNF@/Paper and Cotton_CNF@/Nafion SCs, respectively. All G-CD curves show nearly 100% of columbic efficiency, which was obtained as the ratio of charging and discharging times. It should be noted that high columbic efficiency in SCs corresponds to excellent full reversible Faradaic and capacitive processes. At this respect in particular, the high columbic efficiency observed is unexpected considering that cotton based positive electrodes are made with pseudocapacitive MnO_2 (70 wt% of the total loading of positive electrodes).

It must be pointed out that this surprising good behavior was achieved from dip-coating of CNF onto cotton samples followed by different active layers deposition by means of a well-reported procedure [10,42]. It was also surprising the good behavior showed in Figs. 3 and 4, if it is considered that these SCs are not using thin, but rather thick electrodes with high loadings of MnO_2 and ACs materials. Furthermore, the electrodes produced in this study showed both in-plane and through-plane high electronic conductivity, as it is clearly demonstrated by the box-like and triangular-like behaviors of CV and G-CD curves, respectively. In summary, both type of supercapacitors with Nafion-Na ion-exchange membrane and porous separator (impregnated with 1 M Na_2SO_4) showed low through-plane membrane resistances and excellent capacitances in full cell configurations.

3.3. Electrochemical impedance spectroscopy

Additionally, the capacitive and resistive behavior of these asymmetric SCs were further investigated by electrochemical impedance spectroscopy (EIS) performed at open circuit voltage (OCV) condition. Their Nyquist plots of comparison are reported in Fig. 5. In accordance with the results of CV and G-CD already discussed, the SCs exhibited very low areal electrical resistances of 1.06 Ω cm^2 and 1.44 Ω cm^2 for Cotton_CNF@/Paper and Cotton_CNF@/Nafion SCs, respectively. Though these values of resistance are mainly caused by electrolytes, the contribution of the electrodes and interfacial resistances must be not neglected. The inset of Fig. 5 confirms that Cotton_CNF@/Paper SC with liquid electrolyte has lower resistance than Cotton_CNF@/Nafion SC. Both type of SCs confirm good behaviors with an almost vertical line of impedance points on the left side of the plot ($0 < Z' < 50$). We attribute the quasi-ideal capacitive behavior of both SCs to the very fast capacitive and faradaic electron–transferring processes with low electronic resistances occurring in both type of electrodes, although prevalently in the positive electrodes. The presence of two depressed semicircles of small radius at higher frequencies (Inset of Fig. 5) are assigned to the charge transfer resistance (R_{ct}) and contact resistances occurring between electrode/electrolyte interfaces.

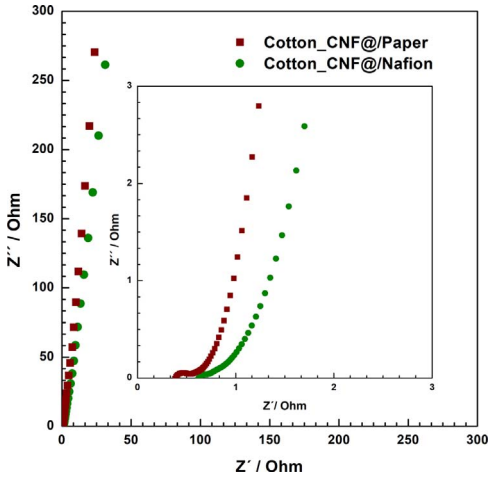

Fig. 5. Nyquist plots of the different hybrid supercapacitors. The inset shows the high-frequency region of impedance.

3.4. Long-term durability tests

The electrochemical characterizations of these hybrid SCs have shown high specific capacitance and a high voltage window of 1.6 V in aqueous electrolyte as it was discussed in previous paragraphs. On the other hand, because of the investigation of their long-term durability is a key point for designing practical SCs devices, a new protocol that combines the usual cycling method, consisting of galvanostatic charge and discharge measurements, with a floating test, which is carried out under constant voltage test at the maximum voltage of 1.6 V during predefined times.

The degradation of symmetric carbon-based SCs under high voltages with Li_2SO_4 electrolyte by using accelerated ageing tests was previously investigated by Beguin et al. [43,44]. They found that gases (e.g., CO_2 and CO) could start to evolve at a cell voltage higher than 1.5 V because the oxidation of carbon materials present in the positive electrodes. They concluded that carbon-based SCs with aqueous 1 M Li_2SO_4 could operate with safety up to 1.5 V, although this value resulted lower than the cell voltage claimed by other similar research study [45]. Noticeably, Beguin et al. used stainless steel collectors instead of the gold collector used in the other study which could explain the different results reported in both investigations.

The accelerated ageing behavior of hybrid supercapacitors based on our proposed cycling and floating method, showed excellent stability for 10k cycles and additional 270 h at constant voltage. The main difference between our proposed method and the usual continuous G-CD is associated to the working condition. Whereas in typical cycling G-CD measurements, the time in which the SC remains at high potentials (e.g. > 1.2 V) is very short, the time in which the SC remains at the maximum voltage (1.6 V) is longer (for hundreds of hours) by using our floating test conditions. Therefore, we believe that this combining cycling and floating method is a better protocol to assess the accelerated aging behavior of developed supercapacitors. The results of cycling test (here not reported) displayed little variations of capacitance with number of cycles showing 105 and 109 F/g at the first cycle for the Cotton_CNF@/Nafion and Cotton_CNF@/paper SCs, respectively and 103 F/g after 10 K cycles for both supercapacitors. The results of the capacitance as function of floating time for the

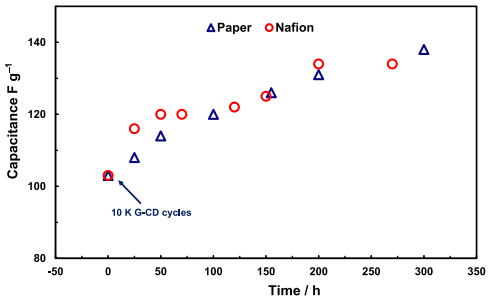

Fig. 6. Capacitance as a function of floating time at 1.6 V for Cotton_CNF@/Paper and Cotton_CNF@/Nafion supercapacitors. The floating test follows 10 K cycles of G-CD at 2 A g^{-1}.

investigated Cotton_CNF@/Paper and Cotton_CNF@/Nafion SCs are reported in Fig. 6.

The floating tests show clearly that the capacitance is increasing with the voltage holding time from about 100 F g^{-1} to 135–140 F g^{-1}, which is an exceptional result for both hybrid MnO_2/AC supercapacitors. Furthermore, it must be remarked that these SCs were tested continuously in cycling and floating condition during several months without any apparent deterioration.

The durability of the two supercapacitors was also monitored through electrochemical impedance spectroscopy (EIS) measurements. In particular, the state-of-health of Cotton_CNF@/Nafion SC was followed by EIS experiments as it is shown in Fig. 7. As it can be seen in Nyquist plots of Fig. 7a (inset), the resistance increases slowly and without jumps throughout floating tests, even at the maximum time of 270 h, which is clearly evidenced along all frequencies. The high Z′ values observed at lower frequencies (left side of Fig. 7a) could be attributed to the enhancement of pseudocapacitance in the positive electrode caused by the increased active surface area of oxides with aging time. Nevertheless, all experimental points at lower frequencies are straight lines sharing practically the same slope. The absence of semi-circles at lower frequencies (from Hz to mHz) indicates that there was not any accentuated Faradaic process during time scale measurement, despite the Cotton_CNF@/Nafion SC must have some redox process in its positive electrode, if it is taken into consideration that $Mn^{4+} \Leftrightarrow Mn^{3+}$ reaction occurs after holding the maximum voltage (1.6 V) to the cell for very long time. On the other hand, there is not any appreciable degradation of the SC as shown in Fig. 7, even with the increase of capacitance previously discussed (Fig. 6). In fact, it must be considered that some degradation occurs for MnO_2 electrodes whenever the operating potential goes above 0.8–1 V (vs normal hydrogen electrode, NHE) due to OER [10,30]. Moreover, it can be noted that our full cell supercapacitors sustained stable performance even when the cell was running at the maximum voltage (i.e. 1.6 V) for hundreds of hours (about 300 h) with unvaried or even increased capacitance performances. It must be also considered that the full cell have to be perfectly sealed, otherwise undesired leakages of electrolyte and water may occur with the subsequent loss of conductivity and performance of the supercapacitor. In summary, SCs with an optimal mass ratio and potential balance between positive and negative electrodes, low resistivity of electrodes and electrolyte, together with absence of electrolyte/water leakages were developed in this study.

The Bode plot, which defines the phase angle for the cell, is presented in Fig. 7b for each stage of characterization; initial, during cycling test and after the voltage-holding conditions. The phase angle (initial) of Cotton_CNF@/Nafion hybrid solid-state supercapacitor is ≈ −84°, very close to −90° of ideal double layer capacitors, though this is a pseudocapacitor that probably shows very fast reversible Faradaic (MnO_2/MnOOH) reactions occurring onto outer surfaces of positive electrode. The phase angle is also indicating that the capacitive behavior is decreasing very slowly from −84° to about −80° (after 270 h) and without considerable deterioration. This is a further demonstration of the exceptional long-term durability of the Cotton_CNF@/Nafion hybrid supercapacitor.

The Fig. 7c reports the real part of impedance versus frequency. It shows long durability with a slight increase of cell resistance with the

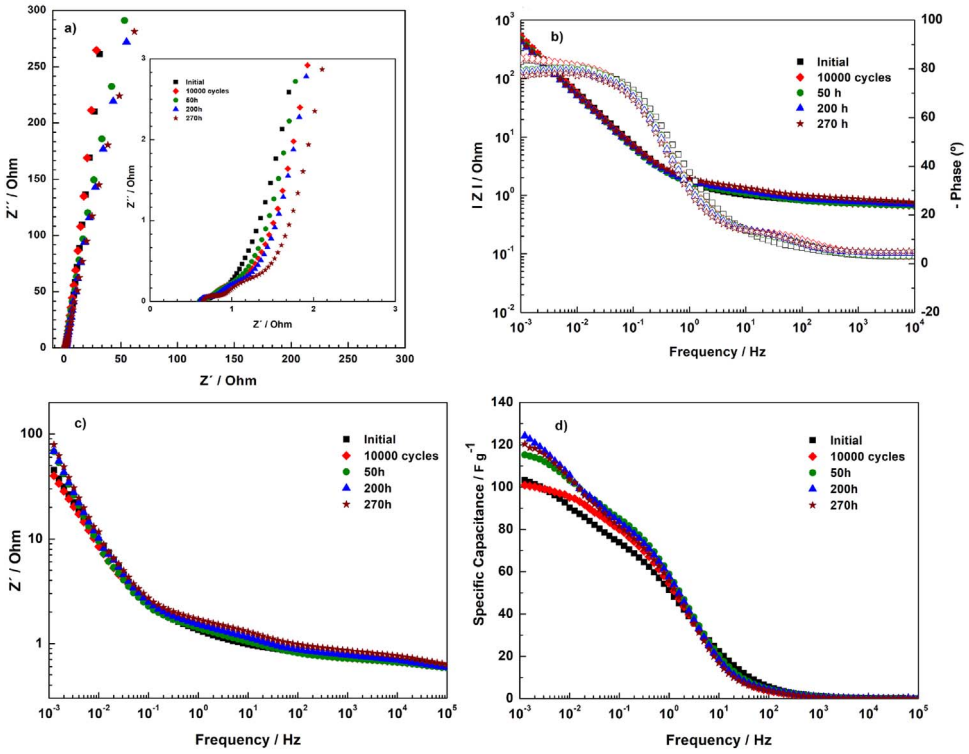

Fig. 7. Long-term durability tests of Cotton_CNF@/Nafion hybrid solid-state supercapacitor. (a) Nyquist plot: the inset plot shows the high-frequency region; (b) Bode plot: absolute impedance (solid symbol), phase angle (open symbol); (c) Real impedance versus frequency; (d) Specific capacitance versus frequency.

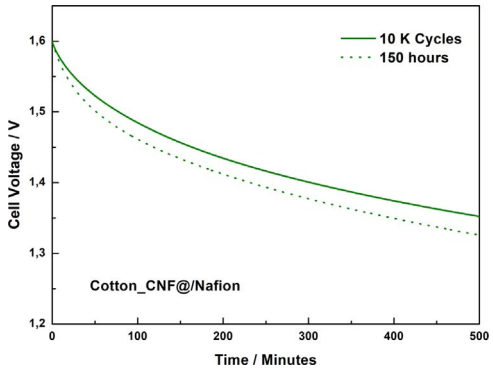

Fig. 8. Self-discharge behaviour of hybrid solid-state Cotton_CNF@/Nafion SC at two different conditions cycling and floating during long-term durability test.

progression of cycling and floating tests at the maximum voltage of 1.6 V. In particular, the initial cell areal resistance increased from 1.44 to 1.84 Ω cm^2, which means an increase of nearly 30% after 10k cycles and 270 h of floating. The resistance values were detected at 2 kHz, a region of high frequency where the ionic resistance of ion conducting membranes is generally measured [46,47]. The increase of capacitance (28%) observed during the long-term durability test (cycling and floating test), can be ascribed, first to an enhancement of pseudocapacitance of the positive electrode, and second because the electrolyte could reach the inner parts of electrodes during the progression of the test. These reasons were supported from the fact that during endurance tests, the distributed resistance as function of frequency observed in Fig. 7a and c showed minor rises, furthermore unwanted jumps of resistance were not observed. This is a further confirmation of the very stable performance of the SCs developed in this study, despite the very harsh conditions of the floating tests considered. On the other hand, EIS results collected during cycling and floating tests, showed in Fig. 7, can be considered as a very interesting method for future studies to monitor the ageing behavior and long-life performance of asymmetric and hybrid SCs.

Galvanostatic charge–discharge measurement is the usual technique to determine specific capacitances at different current rates (e.g. ranges from 0.1 to 5 or 10 A g^{-1}) as those reported in Fig. 4. However, capacitance may be also derived from EIS analysis, as it is shown in Fig. 7d, by using the expression C = [((−1/(2π·f·Z′′))/m) × 4], where m is the total active mass of electrodes. In Fig. 7d, a continuous increase of capacitance with the decrease of frequency is observed until a plateau is reached near 1 mHz. As it was also observed in Fig. 6, the specific capacitance with the endurance floating test increased from 103 to 134 F g^{-1} after 270 h, which corresponds to an increase of 30%, slightly higher than that calculated from EIS (about 21%). The lower capacitance value 121 F g^{-1} at 1 mHz by EIS (Cotton_CNF@/Nafion SC), compared to 134 F g^{-1}, measured by G-CD at 0.2 A g^{-1}, is ascribed to the intrinsic difference between the two methods, which are based on alternate (AC) and direct (DC) current, respectively. Furthermore, it is worth to be noted that capacitance calculated by EIS analysis is derived from a differential method at OCV condition; whereas the capacitance calculated by G-CD analysis is obtained from the discharge curve (from 1.6 to 0 V) of the completely charged SC. Difference in capacitances measured from the methods observed in this study is a topic of discussion in literature [48]. It must be also added that the slight increase of specific capacitance observed from the first of 10k cycles and at the end of floating test (270 h in Fig. 7d), can be explained by considering that there is a minimum time so that electrolyte ions gain access to deeper electrode regions during cycling test, whereas more stable condition are reached during the floating test. Therefore, it is noteworthy that EIS represents a powerful in-situ technique, which can not only explore the electrochemical performance but also allows to monitor the SoH of energy storage devices during long-term durability tests.

Table 3
XP results of C1s and Mn 2p3/2 spectral fitting parameters: binding energy (eV) and percentage of total area for the fresh and aged electrodes.

	C 1s						Mn 2p				
Peak	Peak 1	Peak 2	Peak 3	Peak 4	Peak 5	Peak 1	Peak 2	Peak 3	Peak 4	Peak 5[a]	Peak 6[a]
BE (eV)	284.3 (±0.2)	284.8 (±0.4)	286 (±0.4)	288.2 (±0.6)	290.2 (±0.4)	640.4 (±0.4)	641.3 (±0.2)	641.8 (±0.2)	642.3 (±0.2)	643.7 (±0.2)	645.7 (±0.2)
Functional group/ compound (valence)	C-C sp^2	C-C sp^3 -CH_2-	C-O ether, phenol	C=O carbonyl	-CF_2- PVDF	MnO (II)	Mn_3O_4 (II,III)	MnOOH (III)	MnO_2 (IV)	MnO_2 (IV)	MnO_2 (IV)
Mn oxide fresh electrode(at%)	24	23.3	31.1	6.2	11.3	12.3	4.9	–	49.4	21.5	11.9
Mn oxide aged electrode (+ 270 h) Cotton_CNF@ /Nafion(at%)	32.7	17.7	15.1	13.1	17.8	16.3	–	9.8	42.9	16.4	14.5
Mn oxide aged electrode (> 300 h) Cotton_CNF@ /Paper(at%)	21.5	29.9	19.3	14.1	12.9	14.8	–	9.1	43.3	18.7	14.2

[a] Additional peaks are due to binding energy shifts and attributed to multiplet splitting structures

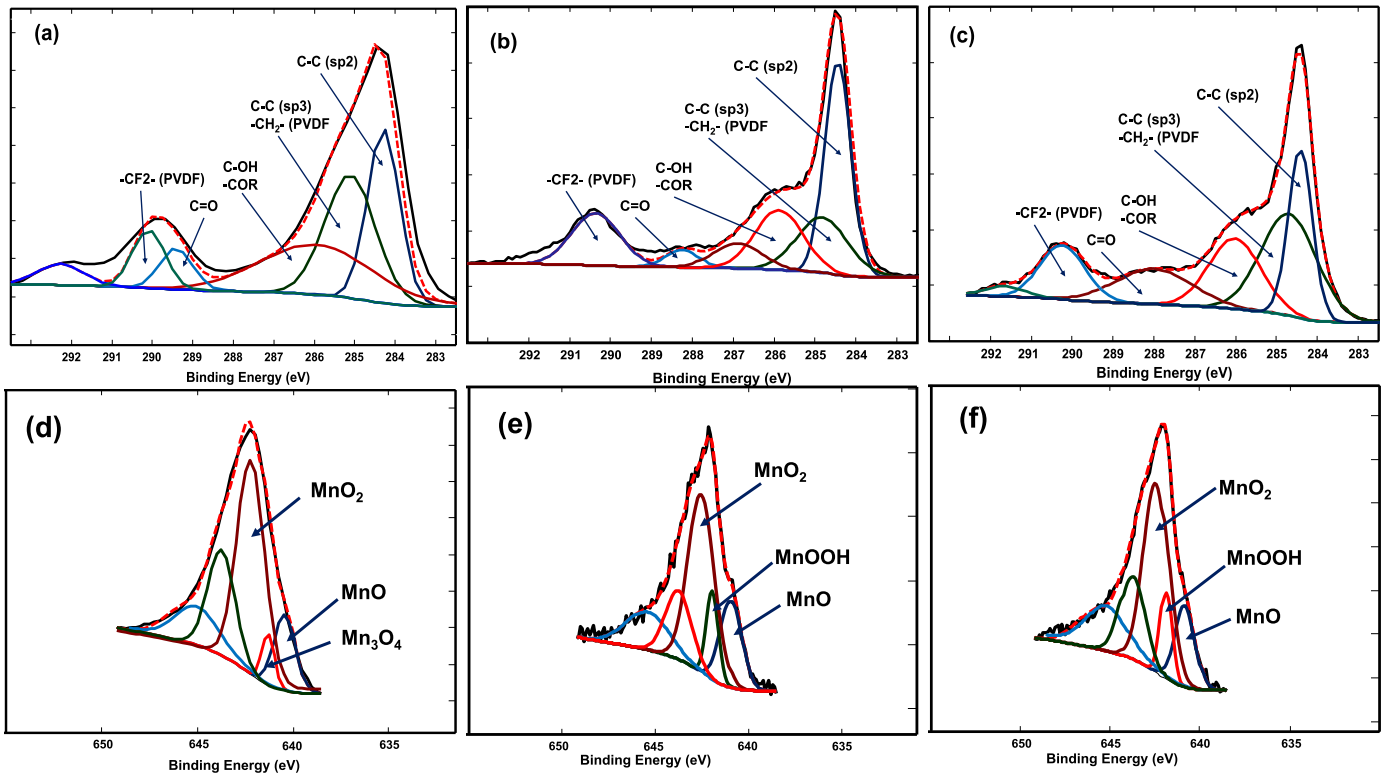

Fig. 9. C1s (top) and Mn $2P_{3/2}$ (bottom) XP-spectra of Cotton_CNF@/Paper and Cotton_CNF@/Nafion SCs. (a), (d) show XP spectra of fresh positive electrode; (b), (e) aged Cotton_CNF@/Nafion electrode; (c), (f) aged Cotton_CNF@/Paper electrode.

In addition to capacitance performance and durability, self-discharge is also another important feature that must be taken into account before developing a proof-of-concept of SCs. In general, self-discharge in SCs can be reduced by using high-purity materials for their electrodes and electrolytes. In this regard, the effects of surface chemistry modification and redox couple characteristics of impurities in electrodes can also condition their self-discharge. On the other hand, self-discharge rates depend on how the supercapacitor has been previously charged, because sometimes charge redistribution will occur for very fast charging. The quantification of charge time is not an easy task, and though 2/3 h of charging is considered a time enough long for the full charge of the supercapacitor, recharge time up to 24 h should be preferred. A detailed review on mechanisms of self-discharge and the suppression of the leakage current was recently discussed in literature [38]. Moreover, it is well recognized that self-discharge rate of SCs is higher than Li-ion batteries [49,50], and higher for aqueous than for non-aqueous SCs [51]. Therefore, self-discharge investigation is an important feature for a better understanding of the developed hybrid solid-state SCs. Fig. 8 shows two different self-discharge curves (after cycling and floating) as function of time after that the Cotton_CNF@/Nafion SC has been charged at 1.6 V for 3 h. The reduced self-discharge rate with a slight voltage decrease over time indicates very promising results, without forgetting the high specific capacitance and exceptional long-term durability demonstrated by these SCs. On the other hand, the reduced self-discharge behaviors observed may come from various contributions such as parasitic faradaic reactions, charge re-distribution, corrosion processes, ion transport limitations and ohmic leakages or even several of these contributions combined [38,51,52]. Furthermore, their identification becomes also difficult, because in a full cell the self-discharge behavior can derive from either electrodes or electrolyte. On the other hand, the charging time at 1.6 V considered (3 h) should be enough to exclude charge re-distribution contribution so it may be supposed that parasitic faradaic reactions are the main cause of the voltage decay of the charged cell [53].

3.5. X-ray photoelectron spectroscopy analysis

After long-durability measurements, cell were disassembly and their relevant components were analysed by XPS, which was carried out on fresh (unaged electrodes) and aged Cotton_CNF@/Paper and Cotton_CNF@/Nafion SCs electrodes to distinguish chemical changes on the surfaces in the electrodes before and after aging (as shown in Table 3).

The analysis of AC layers of aged negative electrodes does not show any appreciable degradation by detecting their C1s spectra. While the XP C1s spectra of unaged and aged positive electrodes show that, some carbon material (i.e. CNF, graphite fiber and carbon black) is slightly modified because of appearance of a shoulder at a binding energy of around 286 eV as shown in Fig. 9.

The C1s spectra of aged samples display a moderate degree of carbon surface oxidation. The oxygenated-functional groups appearing on carbon surfaces are assigned to aromatic C-C (sp^2 hybridization) peak 1 (284.3 ± 0.2 eV); aliphatic C-C (sp^3 hybridization) peak 2 (284.8 ± 0.4 eV); hydroxyl or phenol groups C-O, ethers C-O-R peak 3 (286 ± 0.4 eV); carbonyl C=O peak 4 (288.2 ± 0.2 eV), and fluorine–carbon (-CF_2-) peak 5 (290.2 ± 0.4 eV) by PVDF [40,41]. The presence of Mn^{4+} (MnO_2), Mn^{3+} (MnOOH) and Mn^{2+} (MnO) compounds in aged positive electrodes (Fig. 9e and f) have been clearly identified, and show that likely consecutives redox processes occur in supercapacitors during long-term charge/discharge tests. Though, C1s spectra of aged positive electrodes displays the appearance of oxygen functionalities on carbon surface, the contribution of these species to pseudocapacitance by Faradaic redox process is minimal in neutral aqueous electrolyte (e.g. Na_2SO_4), but considerable in strong acids and bases (e.g. H_2SO_4 and KOH) [54,55]. Besides, XP spectra of discharged electrodes demonstrates the presence of multiple elements in survey analysis such as C, Mn, O, F, S and Na and their compounds. The presence of Na and S are attributed to Na_2SO_4 electrolyte; while oxygen content is ascribed to metal oxides, oxygenated functional groups on carbon electrodes and Na_2SO_4. The fluorine present on electrodes is attribu-

Table 4
Performance comparison of our supercapacitors with other symmetric and asymmetric flexible supercapacitors.

Materials	Electrolyte	SC type	Separator	Working voltage (V)	Capacitance (F/g)	Energy density (Wh/Kg)	Retention	Ref.
SWCNT + MnO_2	2 M Li_2SO_4	Symmetric	Cotton	0.8	170 @ 1 mA/cm^2	–	100% 35 K cycles	[17]
AC	1 M Na_2SO_4	Symmetric	PTFE	1	85 @ 0.25 A/g	–	–	[18]
AC	1 M Li_2SO_4	Symmetric	PTFE	1	90 @ 0.25 A/g	–	92% 10 K cycles	[18]
GO	2 M $EMIMBF_4$/acetonitrile	Symmetric	Cotton	2	18.3 @ 0.1 A/g	12.3	93% 1.5 K cycles	[19]
GO	6 M KOH	Symmetric	Cotton	1	–	7.13	93.8% 1.5 K cycles	[19]
Ni + MWCNT + rGO	5 M LiCl	Symmetric	Cotton	0.8	262 @ 0.84 A/g	–	118% 10 K cycles	[21]
PPy + MO	2 M NaCl	Symmetric	–	0.8	325 @ 1 A/g	24.7	63% 500 cycles	[23]
ACTs* + ACTs*/MnO_2	1 M Na_2SO_4	Asymmetric	Whatman filter paper	2	120 @ 1 mA/cm^2	16.7**	97.5% 1 K cycles	[14]
$NiCo_2O_4$ /ACTs + $NiCo_2O_4$@$NiCo_2O$/ ACTs	PVA/KOH	Asymmetric	Gel Membrane	1.6	60 @ 100 mA/cm^2	21.3**	100% 1 K cycles	[24]
MnO_2/porous carbon cloth (TCC) + TCC	PVA/LiCl	Asymmetric	Gel membrane	2.0	178@ 4 mA/cm^2	25	96% 20 K cycles	[26]
MnO_2/carbon fabric + Fe_2O_3/ carbon fabric	PVA/LiCl	Asymmetric	Gel membrane	1.6	91.3 @ 2 mA/cm^2	32.5	Fair good stability 5 K cycles	[25]
MnO_2/CNF paper +Bi_2O_3/CNF paper	1 M Na_2SO_4	Asymmetric	Filter paper	1.8 V	100.8 @ 1.5 mA/cm^2	11.3	85% 4 K cycles	[27]
CNF + AC + MnO_2	1 M Na_2SO_4	Asymmetric	Porous Paper	1.6	138 @ 0.5 A/g	12.4	130% 10 K cycles + (300 h @ 1.6 V)	This work
CNF + AC + MnO_2	Nafion + Na^+ /1 M Na_2SO_4	Asymmetric	Nafion	1.6	134 @ 0.5 A/g	12	125% 10 K cycles + (270 h @ 1.6 V)	This work

* Carbon active textile; ** Energy density is derived from capacitance of single electrodes.

table to PVDF binder and therefore is irrelevant for the capacitance features of aged electrodes. In order to observe the differences of fresh (unaged) and aged positive electrodes, representative Mn 2p and O 1s spectra were used to detect the major oxygen-based components. However, because oxygen may derive from multiple components such as Na_2SO_4, H_2O, oxygen-based functional groups on carbon surfaces and MnO_x, the O 1s spectra cannot be used with confidence to quantify the contribution of different metal oxide species (i.e. MnO_2, MnOOH and MnO) present in discharged electrodes. Therefore, Mn $2p_{3/2}$ spectra was used to discern three major components in aged samples MnO_2, MnOOH and MnO as reported in Fig. 9 and Table 3. Multiple peaks are assigned to these oxides [56–58], though due to the multiplet-splitting components of Mn 2p (IV) arises when an atom contains unpaired d electrons, Mn (III) and Mn(IV) species have to be added [56,58,59]. The main peak of manganese oxide appears at the binding energy of 542.3 ± 0.2 eV, which corresponds to MnO_2 (IV) with about 43%, and other Mn $2p_{3/2}$ peaks consist of two components with values of 640.4 eV (Mn^{II}) and 641.8 eV (MnOOH).

The comparison of electrochemical performance of SCs developed in this study with other cotton-based electrodes and SCs produced from top-down approach reported in literature is summarized in Table 4. The electrochemical properties of both SCs produced in this study are rather remarkable compared to similar symmetric and asymmetric SCs reported previously. However, self-discharge study and long durability tests with such a harsh conditions, as those performed in this study, have not yet been reported in literature.

Summarizing, the Cotton_CNF@/Nafion SC exhibited specific capacitance of 134 F g^{-1} (at 0.5 A g^{-1}) and energy density of 12 Wh kg^{-1} at voltage of 1.6 V. This SC achieved a maximum power density of 29 kW kg^{-1} with a resistance of 1.84 Ω cm^2. The Cotton_CNF@/paper SC showed a capacitance of 138 F g^{-1}, energy density 12.3 Wh kg^{-1} and areal resistance of 1.38 Ω cm^2. All of these results have been achieved after long-term durability tests.

4. Conclusions

In this study, the design of novel hybrid solid-state asymmetric supercapacitors inspired by the top-down approach starting from a common cotton woven fabric is shown and their properties investigated. The textile-based supercapacitors have exhibited a stable performance in aqueous environment for the voltage range of 0–1.6 V, low self-discharge rates, and very interesting capacitive performance of 138 and 134 F g^{-1} with the porous paper and Nafion membrane, respectively. These values are in the same range of other similar investigations, but obtained with more simple and cheaper materials (carbon nanofibers, activated carbon, graphite fibres, carbon black and dry powder manganese oxide), and with very simple methodologies (dip-coating for a first conductive layer, with a subsequent second active layer based on a slurry of different compositions). Furthermore, we have considered the combination of two methods (cycling and floating) for studying the long-term durability tests of SCs. In particular, this floating methodology utilizes much more harsh conditions than the common cycling based on G-CD tests at high discharge currents so our SCs were subjected to very stressful conditions. In this regard, a slow increase of capacitance of nearly 30%, during long durability floating test for more than 270 h at constant voltage of 1.6 V, was observed. The solid-state hybrid SC showed also very low self-discharge rates even after long-term durability tests. This floating method of characterization can be used as a very interesting strategy to simulate an accelerated aging behavior and in last term to investigate the behavior of real wearable energy storage devices. Another important finding of this study is the demonstration of the stable working voltage at 1.6 V achieved by both SCs, i.e. above the potential of water decomposition (1.23 V), without appreciable evidence of O_2 evolution and MnO_2 degradation processes in the positive electrodes. In this regard, despite the operating cell voltage (1.6 V) is

above this thermodynamic potential (1.23 V) the previously mentioned processes are kinetically sluggish and they do not seem very significant even after the prolonged durability tests performed for hundreds of hours at high voltage.

Acknowledgments

This work was partly financed by FEDER funds through the Competitivity Factors Operational Programme - COMPETE and by national funds through FCT – Foundation for Science and Technology (project POCI-01-0145-FEDER-007136). A.J. Paleo acknowledges the European COST Action CA15107- Multi-Functional Nano-Carbon Composite Materials Network (MultiComp) for its support with a Short Term Scientific Mission (STSM) grant at CNR-ITAE of Messina. The authors would like to thank Dr. Gaetano Squadrito (CNR-ITAE) for morphology study by SEM, Mr. Giuseppe Monforte (CNR-ITAE) for the XPS surface analysis, Dr. Eliana Vieira (CMEMS UMinho) for electrical resistivity analysis and Mr. André Paiva (2C2T UMinho) for helping with graphic design.

References

[1] D. Pech, M. Brunet, H. Durou, P. Huang, V. Mochalin, Y. Gogotsi, P.L. Taberna, P. Simon, Ultrahigh-power micrometre-sized supercapacitors based on onion-like carbon, Nat. Nanotechnol. 5 (2010) 651–654.
[2] J. Chen, K. Sheng, P. Luo, C. Li, G. Shi, Graphene hydrogels deposited in nickel foams for high-rate electrochemical capacitors, Adv. Mater. 24 (2012) 4569–4573.
[3] J. Lin, C. Zhang, Z. Yan, Y. Zhu, Z. Peng, R.H. Hauge, D. Natelson, J.M. Tour, 3-dimensional graphene carbon nanotube carpet-based microsupercapacitors with high electrochemical performance, Nano Lett. 13 (2013) 72–78.
[4] P. Simon, Y. Gogotsi, Materials for electrochemical capacitors, Nat. Mater. 7 (2008) 845–854.
[5] B.E. Conway, W.G. Pell, Double-layer and pseudocapacitance types of electrochemical capacitors and their applications to the development of hybrid devices, J. Solid State Electrochem. 7 (2003) 637–644.
[6] L. Pan, K.X. Wang, X.D. Zhu, X.M. Xie, Y.T. Liu, Hierarchical assembly of SnO2 nanowires on MnO2 nanosheets: a novel 1/2D hybrid architecture for high-capacity, reversible lithium storage, J. Mater. Chem. A 3 (2015) 6477–6483.
[7] C. Xu, F. Kang, B. Li, H. Du, Recent progress on manganese dioxide based supercapacitors, J. Mater. Res. 25 (2010) 1421–1432.
[8] L. Athouël, F. Moser, R. Dugas, O. Crosnier, D. Bélanger, T. Brousse, Variation of the MnO2 birnessite structure upon charge/discharge in an electrochemical supercapacitor electrode in aqueous Na2SO 4 electrolyte, J. Phys. Chem. C 112 (2008) 7270–7277.
[9] T.H. Wu, D. Hesp, V. Dhanak, C. Collins, F. Braga, L.J. Hardwick, C.C. Hu, Charge storage mechanism of activated manganese oxide composites for pseudocapacitors, J. Mater. Chem. A 3 (2015) 12786–12795.
[10] P. Staiti, F. Lufrano, Investigation of polymer electrolyte hybrid supercapacitor based on manganese oxide-carbon electrodes, Electrochim. Acta 55 (2010) 7436–7442.
[11] C. Yu, C. Masarapu, J. Rong, B. Wei, H. Jiang, Stretchable supercapacitors based on buckled single-walled carbon nanotube macrofilms, Adv. Mater. 21 (2009) 4793–4797.
[12] C. Meng, C. Liu, L. Chen, C. Hu, S. Fan, Highly flexible and all-solid-state paperlike polymer supercapacitors, Nano Lett. 10 (2010) 4025–4031.
[13] X. Feng, N. Chen, J. Zhou, Y. Li, Z. Huang, L. Zhang, Y. Ma, L. Wang, X. Yan, Facile synthesis of shape-controlled graphene-polyaniline composites for high performance supercapacitor electrode materials, New J. Chem. 39 (2015) 2261–2268.
[14] H. Li, J. Song, L. Wang, X. Feng, R. Liu, W. Zeng, Z. Huang, Y. Ma, L. Wang, Flexible all-solid-state supercapacitors based on polyaniline orderly nanotubes array, Nanoscale 9 (2017) 193–200.
[15] U. Gulzar, S. Goriparti, E. Miele, T. Li, G. Maidecchi, A. Toma, F. De Angelis, C. Capiglia, R.P. Zaccaria, Next-generation textiles: from embedded supercapacitors to lithium ion batteries, J. Mater. Chem. A 4 (2016) 16771–16800.
[16] L. Bao, X. Li, Towards textile energy storage from cotton T-shirts, Adv. Mater. 24 (2012) 3246–3252.
[17] J. Ren, Y. Zhang, W. Bai, X. Chen, Z. Zhang, X. Fang, W. Weng, Y. Wang, H. Peng, Elastic and wearable wire-shaped lithium-ion battery with high electrochemical performance, Angew. Chem. Int. Ed. 53 (2014) 7864–7869.
[18] S. Seyedin, M.S. Romano, A.I. Minett, J.M. Razal, Towards the knittability of graphene oxide fibres, Sci. Rep. 5 (2015).
[19] L. Hu, M. Pasta, F. La Mantia, L. Cui, S. Jeong, H.D. Deshazer, J.W. Choi, S.M. Han, Y. Cui, Stretchable, porous, and conductive energy textiles, Nano Lett. 10 (2010) 708–714.
[20] K. Jost, C.R. Perez, J.K. McDonough, V. Presser, M. Heon, G. Dion, Y. Gogotsi, Carbon coated textiles for flexible energy storage, Energy Environ. Sci. 4 (2011) 5060–5067.
[21] W.W. Liu, X.B. Yan, J.W. Lang, C. Peng, Q.J. Xue, Flexible and conductive nanocomposite electrode based on graphene sheets and cotton cloth for supercapacitor, J. Mater. Chem. 22 (2012) 17245–17253.
[22] Y. Li, K. Ye, K. Cheng, J. Yin, D. Cao, G. Wang, Electrodeposition of nickel sulfide on graphene-covered make-up cotton as a flexible electrode material for high-performance supercapacitors, J. Power Sources 274 (2015) 943–950.
[23] Y. Yang, Q. Huang, L. Niu, D. Wang, C. Yan, Y. She, Z. Zheng, Waterproof, ultrahigh areal-capacitance, wearable supercapacitor fabrics, Adv. Mater. 29 (2017).
[24] Q. Huang, L. Liu, D. Wang, J. Liu, Z. Huang, Z. Zheng, One-step electrospinning of carbon nanowebs on metallic textiles for high-capacitance supercapacitor fabrics, J. Mater. Chem. A 4 (2016) 6802–6808.
[25] J. Xu, D. Wang, L. Fan, Y. Yuan, W. Wei, R. Liu, S. Gu, W. Xu, Fabric electrodes coated with polypyrrole nanorods for flexible supercapacitor application prepared via a reactive self-degraded template, Org. Electron.: Phys. Mater. Appl. 26 (2015) 292–299.
[26] Z. Gao, N. Song, Y. Zhang, X. Li, Cotton textile enabled, all-solid-state flexible supercapacitors, RSC Adv. 5 (2015) 15438–15447.
[27] P. Yang, Y. Ding, Z. Lin, Z. Chen, Y. Li, P. Qiang, M. Ebrahimi, W. Mai, C.P. Wong, Z.L. Wang, Low-cost high-performance solid-state asymmetric supercapacitors based on MnO2 nanowires and Fe2O3 nanotubes, Nano Lett. 14 (2014) 731–736.
[28] H. Wang, C. Xu, Y. Chen, Y. Wang, MnO2 nanograsses on porous carbon cloth for flexible solid-state asymmetric supercapacitors with high energy density, Energy Storage Mater. 8 (2017) 127–133.
[29] H. Xu, X. Hu, H. Yang, Y. Sun, C. Hu, Y. Huang, Flexible asymmetric micro-supercapacitors based on Bi2O3 and MnO2 nanoflowers: larger areal mass promises higher energy density, Adv. Energy Mater. 5 (2015) 1401882.
[30] V. Khomenko, E. Raymundo-Piñero, F. Béguin, Optimisation of an asymmetric manganese oxide/activated carbon capacitor working at 2 v in aqueous medium, J. Power Sources 153 (2006) 183–190.
[31] T.H. Wu, Y.H. Chu, C.C. Hu, L.J. Hardwick, Criteria appointing the highest acceptable cell voltage of asymmetric supercapacitors, Electrochem. Commun. 27 (2013) 81–84.
[32] A.J. Paleo, V. Sencadas, F.W.J. Van Hattum, S. Lanceros-Méndez, A. Ares, Carbon nanofiber type and content dependence of the physical properties of carbon nanofiber reinforced polypropylene composites, Polym. Eng. Sci. 54 (2014) 117–128.
[33] L. Demarconnay, E. Raymundo-Piñero, F. Béguin, Adjustment of electrodes potential window in an asymmetric carbon/MnO 2 supercapacitor, J. Power Sources 196 (2011) 580–586.
[34] D. Pavlov, Lead-Acid Batteries: Science and Technology (2011), 2011.
[35] M. Armand, J.M. Tarascon, Building better batteries, Nature 451 (2008) 652–657.
[36] A.K. Shukla, S. Venugopalan, B. Hariprakash, Secondary batteries – nickel systems | nickel–cadmium: overview A2, in: Jürgen Garche (Ed.)Encyclopedia of Electrochemical Power Sources, Elsevier, Amsterdam, 2009, pp. 452–458.
[37] G. Hasegawa, K. Kanamori, T. Kiyomura, H. Kurata, T. Abe, K. Nakanishi, Hierarchically porous carbon monoliths comprising ordered mesoporous nanorod assemblies for high-voltage aqueous supercapacitors, Chem. Mater. 28 (2016) 3944–3950.
[38] I.S. Ike, I. Sigalas, S. Iyuke, Understanding performance limitation and suppression of leakage current or self-discharge in electrochemical capacitors: a review, Phys. Chem. Chem. Phys. 18 (2015) 661–680.
[39] L. Chen, H. Bai, Z. Huang, L. Li, Mechanism investigation and suppression of self-discharge in active electrolyte enhanced supercapacitors, Energy Environ. Sci. 7 (2014) 1750–1759.
[40] R. Larciprete, S. Gardonio, L. Petaccia, S. Lizzit, Atomic oxygen functionalization of double walled C nanotubes, Carbon 47 (2009) 2579–2589.
[41] F. Lufrano, P. Staiti, Influence of the surface-chemistry of modified mesoporous carbon on the electrochemical behavior of solid-state supercapacitors, Energy Fuels 24 (2010) 3313–3320.
[42] P. Staiti, F. Lufrano, Study and optimisation of manganese oxide-based electrodes for electrochemical supercapacitors, J. Power Sources 187 (2009) 284–289.
[43] P. Ratajczak, K. Jurewicz, F. Béguin, Factors contributing to ageing of high voltage carbon/carbon supercapacitors in salt aqueous electrolyte, J. Appl. Electrochem. 44 (2014) 475–480.
[44] E. Frackowiak, P. Ratajczak, F. Béguin, Electrochemical capacitors based on carbon electrodes in aqueous electrolytes, Adv. Electrochem. Sci. Eng. (2016) 285–312.
[45] K. Fic, G. Lota, M. Meller, E. Frackowiak, Novel insight into neutral medium as electrolyte for high-voltage supercapacitors, Energy Environ. Sci. 5 (2012) 5842–5850.
[46] F. Müller, C.A. Ferreira, D.S. Azambuja, C. Alemán, E. Armelin, Measuring the proton conductivity of ion-exchange membranes using electrochemical impedance spectroscopy and through-plane cell, J. Phys. Chem. B 118 (2014) 1102–1112.
[47] X.Z. Yuan, C. Song, H. Wang, J. Zhang, Electrochemical Impedance Spectroscopy in PEM Fuel Cells: Fundamentals and Applications (2010), 2010.
[48] E.P. Randviir, C.E. Banks, Electrochemical impedance spectroscopy: an overview of bioanalytical applications, Anal. Methods 5 (2013) 1098–1115.
[49] X. Luo, J. Wang, M. Dooner, J. Clarke, Overview of current development in electrical energy storage technologies and the application potential in power system operation, Appl. Energy 137 (2015) 511–536.
[50] L. Weinstein, R. Dash, Supercapacitor carbons: have exotic carbons failed?, Mater. Today 16 (2013) 356–357.
[51] F. Béguin, E. Frackowiak, Supercapacitors: Materials, Systems, and Applications (2013), 2013.
[52] H.A. Andreas, Self-discharge in electrochemical capacitors: a perspective article, J. Electrochem. Soc. 162 (2015) A5047–A5053.
[53] L. García-Cruz, P. Ratajczak, J. Iniesta, V. Montiel, F. Béguin, Self-discharge of AC/AC electrochemical capacitors in salt aqueous electrolyte, Electrochim. Acta 202 (2016) 66–72.

[54] Y.J. Oh, J.J. Yoo, Y.I. Kim, J.K. Yoon, H.N. Yoon, J.H. Kim, S.B. Park, Oxygen functional groups and electrochemical capacitive behavior of incompletely reduced graphene oxides as a thin-film electrode of supercapacitor, Electrochim. Acta 116 (2014) 118–128.
[55] J.W. Lang, X.B. Yan, W.W. Liu, R.T. Wang, Q.J. Xue, Influence of nitric acid modification of ordered mesoporous carbon materials on their capacitive performances in different aqueous electrolytes, J. Power Sources 204 (2012) 220–229.
[56] M.C. Biesinger, B.P. Payne, A.P. Grosvenor, L.W.M. Lau, A.R. Gerson, R.S.C. Smart, Resolving surface chemical states in XPS analysis of first row transition metals, oxides and hydroxides: Cr, Mn, Fe, Co and Ni, Appl. Surf. Sci. 257 (2011) 2717–2730.
[57] S. Ardizzone, C.L. Bianchi, D. Tirelli, Mn3O4 and γ-MnOOH powders, preparation, phase composition and XPS characterisation, Colloids Surf. A: Physicochem. Eng. Asp. 134 (1998) 305–312.
[58] H.W. Nesbitt, D. Banerjee, Interpretation of XPS Mn(2p) spectra of Mn oxyhydroxides and constraints on the mechanism of MnO2 precipitation, Am. Miner. 83 (1998) 305–315.
[59] E.S. Ilton, J.E. Post, P.J. Heaney, F.T. Ling, S.N. Kerisit, XPS determination of Mn oxidation states in Mn (hydr)oxides, Appl. Surf. Sci. 366 (2016) 475–485.